Comput Geosci (2016) 20:421–435
DOI 10.1007/s10596-015-9535-2

ORIGINAL PAPER

Compositional flow modeling using a multi-point flux mixed finite element method

Gurpreet Singh[1] · **Mary F. Wheeler**[1]

Received: 27 September 2014 / Accepted: 25 September 2015 / Published online: 14 October 2015

Abstract We present a general compositional formulation using multi-point flux mixed finite element (MFMFE) method on general hexahedral grids. The mixed finite element framework allows for local mass conservation, accurate flux approximation, and a more general treatment of boundary conditions. The multi-point flux inherent in MFMFE scheme allows the usage of a full permeability tensor. The proposed formulation is an extension of single and two-phase flow formulations presented by Wheeler and Yotov, SIAM J. Numer. Anal. **44**(5), 2082–2106 (2006) with similar convergence properties. Furthermore, the formulation allows for black oil, single-phase and multi-phase incompressible, slightly and fully compressible flow models utilizing the same design for different fluid systems. An accurate treatment of diffusive/dispersive fluxes owing to additional velocity degrees of freedom is also presented. The applications areas of interest include gas flooding, CO_2 sequestration, contaminant removal, and groundwater remediation.

Keywords Compositional flow · Multipoint flux mixed finite element method · General hexahedral grids · CO_2 enhanced oil recovery

✉ Gurpreet Singh
gurpreet@ices.utexas.edu

Mary F. Wheeler
mfw@ices.utexas.edu

[1] Center for Subsurface Modeling, Institute for Computational Engineering and Sciences, POB 5.324, The University of Texas at Austin, Austin, TX 78712, USA

1 Introduction

Compositional flow modeling has been used for simulating CO_2 sequestration, ground water remediation, and contaminant plume migration. In the oil and gas industry, it is widely used for evaluating gas flooding scenarios as a tertiary recovery process. The gas flooding targets achieving either direct miscibility or multi-contact miscibility to counter adverse mobilities to maximize recovery. A number of variants of the above process exist, based upon economical considerations, such as gas slug injection along with a chase fluid or water alternating gas (WAG). The modeling involves solving a system of non-linear equations, invoking a local equilibrium assumption, including an equation of state. This combined with partial differential equations representing mass conservation represent a differential algebraic system which is known for its numerical difficulties. An extensive amount of literature is available which elaborate on different model formulations and solution algorithms to address this problem.

Some of the earliest expositions in compositional flow modeling were carried out by [27] using a fully implicit solution scheme. Coats [6] later presented another implicit formulation where the transmissibility terms (relative permeabilities) were treated implicitly during the construction of Jacobian matrix. A similar formulation with explicit transmissibility terms (relative permeabilities) was presented in [39]. These schemes were later categorized as primary variable switching (PVS) owing to change of primary variables associated with phase appearance and disappearance. A local criteria based upon saturation pressure test is employed to test the stability of the hydrocarbon phase. Here, a phase is assumed to be present only if the phase saturations lie between 0 and 1. Furthermore, the system of partial differential equations associated with

component conservation equations and the algebraic system of equations corresponding to the phase behavior model are solved in a monolithic fashion. Lauser et al. [15] pointed out some of the issues with PVS schemes at near critical conditions for the hydrocarbon fluid phase. The authors used a non-linear complimentarity condition to circumvent the problems associated with phase appearance and disappearance.

A number of sequential solution schemes are discussed in literature ([1, 4, 14, 21]) for solving compositional flow equations. An implicit pressure equation is formulated, with explicit treatment of transmissibility terms, using a volume balance constraint which states pore volume is equal to fluid volume. This is followed by an explicit concentration update. Here, a backward Euler scheme is used, for time-discretization of the PDEs, with respect to the pressure variable (implicit pressure), whereas a forward Euler scheme (time-lagging) is used for the concentration variables (explicit concentration). Note that an implicit or explicit treatment of a term, which can be expressed as a function of the primary variables (pressure and concentrations), implies the time-level associated with the term. This approach was later named implicit pressure explicit concentration (IMPEC) scheme based on the well-known implicit pressure explicit saturation (IMPES) scheme. Watts [32] also presented an extension of the IMPES scheme for compositional flow following [1] in the construction of a pressure equation based upon a volume balance or constraint. Once the pressure equation is solved, the total fluxes are evaluated and then a system of saturation equations are solved explicitly. This is followed by phase flux evaluation and component transport. In all the above approaches, a finite difference method is used for spatial discretization. An iteratively coupled IMPEC scheme is presented by [30] where iterations are performed, between an implicit pressure system and explicit concentration updates, until a desired tolerance is achieved. Here, an RT_0, a mixed finite element scheme (cell-centered finite difference) ([28]), and a second-order DG method were used for spatial discretization of pressure and saturation equations, respectively.

A sequential implicit scheme is an implicit approach that relies upon an inexact Newton method to construct an approximation of the exact Jacobian. A compositional formulation, with mixed methods for pressure and first-order scheme for concentrations, can be found in [16], and [31] where this sequential implicit scheme is used. Hajibeygi and Tchelepi [11] present another compositional formulation where a sequential implicit solution approach is employed along with a finite-volume discretization scheme. In this work, we formulate a similar scheme based on a multi-point flux mixed finite element (MFMFE) method as the discretization. The MFMFE scheme provides accurate and locally mass conservative fluxes and eliminates grid orientation effects owing to gradient in pressure. This scheme allows for a full tensor permeability to capture permeability anisotropy. We also differ in the use of a logically rectangular grid with general hexahedral elements. These elements reduce the number of unknowns when compared to tetrahedral meshes. Furthermore, the general hexahedral elements capture complex reservoir geometries without requiring substantial manipulation of associated petrophysical properties. This also allows for capturing of non-planar fractures [29] as a future prospect for compositional flow modeling in fractured poroelastic reservoirs.

It is also imperative to discuss some of the restrictions placed on phase-behavior modeling owing to a choice of solution algorithms discussed before. The Rachford-Rice (RR) ([26]) equations allows a better treatment of the non-linearities presented by the phase behavior model. The constant-K flash represented by RR equations can be easily reformulated as a constrained optimization problem [20]. The objective function for this minimization problem is known to be convex and therefore robust solution schemes can be utilized [22]. However, the model formulations used in [6, 15] cannot take advantage of this due to the restrictive choice of primary unknowns. For these implicit solution schemes, where the algebraic equations associated with phase behavior model and partial differential equations for the compositional flow model are solved monolithically, phase appearance and disappearance due to near critical fluid phase behavior poses significant problems. For primary variable switching (PVS) schemes, this might introduce oscillations due to frequent changes in the rank of the Jacobian. Whereas, for complementarity condition based method, the Jacobian might become ill-conditioned or rank deficient. The sequential implicit scheme, used in this work, and a few other fully implicit formulations such as variants of method presented by [9], circumvent these issues by solving the algebraic system for phase behavior model equations separately using robust solution algorithms. Another exposition in this direction can be found in [38]. A comparison of different linearization approaches, using finite difference scheme, and the resulting computational costs is presented by [7].

In the sections below, we begin by describing the compositional model formulation along with boundary, initial and closure conditions. This is followed by a description of the hydrocarbon phase behavior model based upon the local equilibrium assumption. Please note that the aqueous phase is assumed to be slightly compressible. For the sake of brevity, we skip directly to the fully discrete formulation where a weak formulation of the problem is presented

along with the associated finite element spaces and quadrature rules. We also briefly discuss the linearization choices leading to the construction of the implicit pressure equation. Finally, we present a number of numerical results comprising of verification and benchmarking cases along with a comparison between two-point flux approximation (TPFA) and MFMFE schemes. We also present two field cases where gas flooding is used as a tertiary recovery process to further demonstrate the model capabilities for complex cases.

2 Compositional model formulation

We begin by describing a continuum description of the compositional model. The general mass balance equation can be written in the differential form (also referred to as the strong form) and is given by Eq. 1,

$$\frac{\partial W_{i\alpha}}{\partial t} + \nabla \cdot F_{i\alpha} - R_{i\alpha} - r_{mi\alpha} = 0. \tag{1}$$

Where $W_{i\alpha}$ is the concentration of component i in phase α, $F_{i\alpha}$ the flux of component i in phase α, $R_{i\alpha}$ the rate of generation/destruction of component i in phase α owing to reactive changes, and $r_{mi\alpha}$ the rate of increase/decrease component i in phase α owing to phase changes. The mass balance Eq. 1 can be expressed in an expanded form given by,

$$\frac{\partial(\epsilon_\alpha \rho_\alpha \xi_{i\alpha})}{\partial t} + \nabla \cdot (\rho_\alpha \xi_{i\alpha} u_\alpha - \epsilon_\alpha D_{i\alpha} \cdot \nabla (\rho_\alpha \xi_{i\alpha})) = \epsilon_\alpha r_{i\alpha} + r_{mi\alpha}. \tag{2}$$

Here, ϵ_α it the volume occupied by phase α, ρ_α the density of phase α, $\xi_{i\alpha}$ the fraction of component i in phase α, and $D_{i\alpha}$ the dispersion tensor. Please note that the equations outlined in this section can have either a mass or molar basis. For the sake of simplicity of model description, the following assumptions are made:

1. Isothermal reservoir conditions.
2. Rock-fluid interactions are neglected, i.e., no sorption processes are considered.
3. Non-reactive flow.

Appying these assumptions to Eq. 2, we obtain Eq. 3.

$$\frac{\partial(\phi S_\alpha \rho_\alpha \xi_{i\alpha})}{\partial t} + \nabla \cdot (\rho_\alpha \xi_{i\alpha} u_\alpha - \phi S_\alpha D_{i\alpha} \cdot \nabla (\rho_\alpha \xi_{i\alpha})) = q_{i\alpha} + r_{mi\alpha} \tag{3}$$

2.1 Component conservation equations

Summing Eq. 3 over the total number of phases (N_p) and noting that $\sum_\alpha r_{mi\alpha} = 0$ results in Eq. 4.

$$\frac{\partial}{\partial t}\left(\sum_\alpha \phi S_\alpha \rho_\alpha \xi_{i\alpha}\right) + \nabla \cdot \sum_\alpha (\rho_\alpha \xi_{i\alpha} u_\alpha - \phi S_\alpha D_{i\alpha} \cdot \nabla (\rho_\alpha \xi_{i\alpha})) = \sum_\alpha q_{i\alpha} \tag{4}$$

The phase fluxes (u_α) are given by Darcy's law,

$$u_\alpha = -K \frac{k_{r\alpha}}{\mu_\alpha} \left(\nabla p_\alpha - \rho_{m,\alpha} g\right). \tag{5}$$

Here, S_α is the saturation of phase α (ratio of volume of phase α to pore volume), ϕ the porosity (ratio of pore volume to bulk volume), $q_{i\alpha}$ the rate of injection of component i in phase α (mass/mole/volume basis), u_α the Darcy flux, and $\rho_{m,\alpha}$ the mass density of phase α. Also let, $N_i = \sum_\alpha \rho_\alpha S_\alpha \xi_{i\alpha}$ and $q_i = \sum_\alpha q_{i\alpha}$ then the component conservation equations can be written as,

$$\frac{\partial}{\partial t}(\phi N_i) + \nabla \cdot F_i - \nabla \cdot \left(\sum_\alpha \phi S_\alpha D_{i\alpha} (\nabla \rho_\alpha \xi_{i\alpha})\right) = q_i. \tag{6}$$

We define component flux F_i as,

$$F_i = -K \sum_\alpha \rho_\alpha \xi_{i\alpha} \frac{k_{r\alpha}}{\mu_\alpha} \left(\nabla p_\alpha - \rho_{m,\alpha} g\right). \tag{7}$$

Rearranging,

$$F_i = -K \Lambda_i \left(\nabla p_{\text{ref}} - \frac{1}{\Lambda_i} \sum_\alpha \rho_\alpha \xi_{i\alpha} \frac{k_{r\alpha}}{\mu_\alpha} \rho_{m,\alpha} g + \frac{1}{\Lambda_i} \sum_{\alpha \neq \text{ref}} \rho_\alpha \xi_{i\alpha} \frac{k_{r\alpha}}{\mu_\alpha} \nabla p_{c\alpha}\right) \tag{8}$$

where,

$$\Lambda_i = \sum_\alpha \rho_\alpha \xi_{i\alpha} \frac{k_{r\alpha}}{\mu_\alpha} \tag{9}$$

In the following text, we will describe a system of partial differential equations associated with component mass conservation (compositional equations) with the reference phase pressure (p_{ref}) and component concentrations (N_i) as the primary variables. We define N_1 as the water component concentration, $\vec{N}_{HC} = N_{2,\ldots,N_c}$ the hydrocarbon component concentration vector and $\vec{N} = N_{1,\ldots,N_c}$ the component concentration vector.

2.2 Boundary and initial conditions

For the sake of convenience of model description, we assume no flow external boundary condition everywhere.

However, this is by no means restrictive and more general boundary conditions can be also be treated.

$$u_\alpha \cdot n = 0 \text{ on } \partial\Omega \tag{10}$$

The initial condition is as follows,

$$p_{\text{ref}} = p^0, \tag{11a}$$

$$N_i = N_i^0. \tag{11b}$$

2.3 Closure and constraints

The phase saturations S_α are calculated as functions of primary variables p_{ref} and $N_{i=1,\ldots,N_c}$ as follows,

$$\begin{aligned} S_w(p_{ref}, N_1) &= \frac{N_w}{\rho_w}, \\ S_o(p_{ref}, \vec{N}_{HC}) &= \frac{(1-\nu)}{\rho_o} \sum_{i=2}^{N_c} N_i, \\ S_g(p_{ref}, \vec{N}_{HC}) &= \frac{\nu}{\rho_g} \sum_{i=2}^{N_c} N_i. \end{aligned} \tag{12}$$

Where ν is the mole fraction of the hydrocarbon gas phase, and o, w, and g represent the hydrocarbon oil, water, and hydrocarbon gas phases, respectively. A saturation constraint exist on phase saturation given by,

$$\sum_\alpha S_\alpha = 1. \tag{13}$$

The capillary pressure is a monotonic and continuous function of reference phase saturation (S_{ref}). The relative permeabilities are continuous functions of reference phase saturation (S_{ref}). A more general table-based capillary pressure and relative permeability curve description has also been implemented.

$$p_{c\alpha}(p_{ref}, \vec{N}) = p_{c\alpha}(S_{ref}) = p_\alpha - p_{\text{ref}} \tag{14}$$

Furthermore, a slightly compressible Eq.15a and cubic equation of state Eq. 15b are used for water and hydrocarbon phases, respectively.

$$\rho_w(p_{ref}) = \rho_{w,0} exp\left[C_w(p_{\text{ref}} + p_{cw} - p_{\text{ref},0})\right] \tag{15a}$$

$$\rho_\alpha(p_{ref}, \vec{N}_{HC}) = \frac{p_\alpha}{Z_\alpha RT}, \alpha \neq \text{w} \tag{15b}$$

Here, ρ_α is the molar density of phase α and ρ_w the water phase density. The porous rock matrix is assumed to be compressible, with C_r as the rock compressibility, satisfying the following relationship,

$$\phi(p_{ref}) = \phi_0\left[1 + C_r(p_{\text{ref}} - p_{\text{ref},0})\right], \tag{16}$$

where ϕ_0 and $p_{ref,0}$ are constants at the reference state (or standard conditions).

3 Hydrocarbon phase behavior model

The phase behavior modeling for hydrocarbon phases is based upon a local equilibrium assumption. The equilibrium component concentrations are then calculated point wise given a pressure (p_{ref}), temperature (T), and overall mole fraction ($\vec{z}$). A normalization of hydrocarbon component concentrations $\vec{N}_{HC}$ give overall component mole fractions $\vec{z}$.

$$z_i(\vec{N}_{HC}) = \frac{N_i}{\sum_{i=2}^{N_c} N_i} \tag{17}$$

Let $\xi_{i\alpha}$ be the mole fraction of component i in phase α and ν the normalized moles of gas phase, then from mass balance we have,

$$\nu\xi_{ig} + (1-\nu)\xi_{io} = z_i, \tag{18a}$$

$$\sum_{i=2}^{N_c} \xi_{io} = 1, \tag{18b}$$

$$\sum_{i=2}^{N_c} \xi_{ig} = 1. \tag{18c}$$

The partitioning coefficient $\vec{K}^{\text{par}}$ for a component i between hydrocarbon phases is given by,

$$K_i^{\text{par}} = \frac{\xi_{ig}}{\xi_{io}}, \quad i \neq 1. \tag{19}$$

Rearranging the above equations we have,

$$\xi_{io}(\vec{N}_{HC}, \vec{K}^{par}, \nu) = \frac{z_i}{1 + (K_i^{\text{par}} - 1)\nu}, \tag{20a}$$

$$\xi_{ig}(\vec{N}_{HC}, \vec{K}^{par}, \nu) = \frac{K_i^{\text{par}} z_i}{1 + (K_i^{\text{par}} - 1)\nu}. \tag{20b}$$

The equilibrium hydrocarbon component distribution is calculated using Rachford-Rice (RR) equation ([26]) given as,

$$f(\vec{N}_{HC}, \vec{K}^{par}, \nu) = \sum_{i=2}^{N_c} \frac{(K_i^{\text{par}} - 1)z_i}{1 + (K_i^{\text{par}} - 1)\nu} = 0. \tag{21}$$

At equilibrium, the fugacities of a component i are equal in all the phases given by the iso-fugacity criteria Eq. 22.

$$g(p_{ref}, \vec{N}_{HC}, \vec{K}^{par}, \nu) = ln\Phi_{io} - ln\Phi_{ig} - lnK_i^{\text{par}} = 0. \tag{22}$$

Where the fugacity of component i in phase α is given by,

$$ln\Phi_{i\alpha}(p_{ref}, \vec{N}_{HC}, \vec{K}^{par}, \nu) = -C_i + \frac{B_i}{B_\alpha}(\bar{Z}_\alpha - 1) - ln(\bar{Z}_\alpha - B_\alpha) - \frac{A_\alpha}{2\sqrt{2}B_\alpha}\left(\frac{2\sum_{j=2}^{N_c}\xi_{j\alpha}A_{ij}}{A_\alpha} - \frac{B_i}{B_\alpha}\right) ln\left(\frac{\bar{Z}_\alpha + (1+\sqrt{2})B_\alpha}{\bar{Z}_\alpha + (1-\sqrt{2})B_\alpha}\right). \quad (23)$$

Here, $\bar{Z}_\alpha = \bar{Z}_\alpha(p_{ref}, \vec{N}_{HC}, \vec{K}^{par}, \nu)$. For a given pressure ($p_{ref}$) and hydrocarbon composition (N_{HC}) and temperature (T) Eqs. 21 and 22 can be linearized in terms of lnK_i and ν.

$$\begin{pmatrix} \partial f/\partial lnK^{\text{par}} & \partial f/\partial \nu \\ \partial g/\partial lnK^{\text{par}} & \partial g/\partial \nu \end{pmatrix} \begin{pmatrix} \delta \boldsymbol{lnK}^{\text{par}} \\ \delta \nu \end{pmatrix} = \begin{pmatrix} -R_1 \\ -R_2 \end{pmatrix} \quad (24)$$

Eliminating $\delta\nu$ from the linear system,

$$\left(\frac{\partial f}{\partial \boldsymbol{lnK}^{\text{par}}} - \frac{\partial f}{\partial \nu}\left(\frac{\partial g}{\partial \nu}\right)^{-1}\frac{\partial g}{\partial \boldsymbol{lnK}^{\text{par}}}\right)\delta \boldsymbol{lnK}^{\text{par}} = -R_1 + \frac{\partial f}{\partial \nu}\left(\frac{\partial g}{\partial \nu}\right)^{-1} R_2. \quad (25)$$

Since the system under consideration is highly non-linear with multiple solutions, we must either provide good initial guesses or constraint the system appropriately so as to get a unique solution. The hydrocarbon phase behavior model is a global optimization problem and therefore relies upon providing a good initial estimates for $\vec{K}^{\text{par}}$ and ν based upon heuristics. The Wilson's equation ([37]) (26) is an empirical correlation which provides initial guesses for $K_i^{\text{par}}s$.

$$K_i^{\text{par}} = \frac{1}{p_{ri}} exp\left[5.37(1+\omega_i)\left(1 - \frac{1}{T_{ri}}\right)\right] \quad (26)$$

Using these partitioning coefficients (K_i^{par}) and the given composition (z_i) (21) is then solved to get an initial estimate for ν. We use three different ways of determining phase stability and consequently the compositions of unstable phases using iso-fugacity flash calculations. The three methods differ either in the calculation of initial estimates of K_i^{par}s or the determination of phase stability (negative flash vs. tangent plane distance). However, the primary unknowns and equations for the three methodologies are the same as presented in this section.

For non-polar molecules (hydrocarbons), a Peng-Robinson cubic equation of state ([24]) empirically correlates pressure, temperature, and molar volume. The values of Z_α are calculated using this cubic equation of state, given in the Appendix (51). For given pressure, temperature, composition ($\vec{n}$), partitioning coefficients ($\vec{K}^{\text{par}}$), and vapor fraction (ν), the cubic equation of state provides three values of Z_α. A unique solution is obtained by selecting the root which has the minimum Gibb's free energy given by,

$$\left.\frac{\partial G}{\partial n_i}\right|_{\alpha,T,P} = \mu_{i\alpha} = \mu_i^o + RTln\Phi_{i\alpha}, \quad (27a)$$

$$dG|_{\alpha,T,P} = \sum_{i=2}^{N_c}\left.\frac{\partial G}{\partial n_i}\right|_{\alpha,T,P} dn_i = h(Z_\alpha). \quad (27b)$$

Here, μ_i^o represents the reference state and is a different constant for each component. Among the three roots of the cubic EOS, Z_α corresponding to the minimum $dG|_{\alpha,T,P}$ is chosen. The cubic EOS, or alternatively Z_α, is not a part of the Jacobian (50) due to the restriction placed by minimum Gibb's free energy constraint. The algorithm for flash iteration can be outlined as follows:

1. Calculate an initial estimate of K_i^{par}s from Wilson's correlation (26).
2. For a given P, T, $\vec{z}$, and K_i^{par}s calculated above, solve the Rachford-Rice (21) for ν.
3. Calculate $\xi_{i\alpha}$ from Eq. 20.
4. Evaluate Z_α using Eq. 51.
5. Evaluate residuals of fugacity Eq. 22, stop if convergence tolerance is achieved.
6. If tolerance is not achieved, solve (25) for new values of $K_i^{\text{par}}s$.
7. Stop if K_i^{par} is trivial i.e., $K_i^{\text{par}} = 1$.
8. Return to 1.

A tangent plane distance analysis is used to determine phase-stability and the number of stable hydrocarbon phases which was originally presented by [2] and later improved and extended by [18, 19]. Furthermore, a quasi-Newton successive substitution algorithm is used to calculate phase and component mole fractions. An extensive literature is dedicated to the solution algorithms ([8, 10, 12, 17, 23]) associated with phase behavior modeling and a detailed description is therefore curtailed in this paper.

4 Fully discrete formulation

We utilize a multi-point flux mixed finite element method to construct a fully discrete form of the flow problem describe earlier. Multi-point flux mixed finite element methods have been developed by [13, 35] for general hexahedral grids. Mixed finite element methods are preferred over other variational formulations due to their local mass conservation and improved flux approximation properties. An appropriate choice of mixed finite element spaces and degrees of freedom based upon the qudrature rule for

numerical integration ([33, 36]) allow flux degrees of freedoms to be defined in terms of cell-centered gridblock pressures adajacent to the vertex. A 9 and 27 point pressure stencil is formed for logically rectangular 2D and 3D grids, respectively.

4.1 Finite element spaces

Here, we present the appropriate finite element spaces utilized to formulate an MFMFE scheme. An enhanced $BDDF_1$ space on $\hat{E}$,with additional degrees of freedom, for a general hexahedral element is defined on a reference unit cube Eq. 30 by enhancing the $BDDF_1$ space Eq. 28. Here, $BDDF_1$ is the Brezzi-Douglas-Duŕan-Fortin mixed finite element space for second order elliptic problems ([3]). Let, $V = \{v \in H(div;\Omega) : v \cdot n = 0 \text{ on } \partial\Omega^N\}$, $W \equiv L^2(\Omega)$

$$\begin{aligned} BDDF_1(\hat{E}) &= P_1(\hat{E})^3 + r_0 curl(0,0,\hat{x}\hat{y}\hat{z})^T + r_1 curl(0,0,\hat{x}\hat{y}^2)^T \\ &\quad + s_0 curl(\hat{x}\hat{y}\hat{z},0,0)^T + s_1 curl(\hat{y}\hat{z}^2,0,0)^T \\ &\quad + t_0 curl(0,\hat{x}\hat{y}\hat{z},0)^T + t_1 curl(0,\hat{x}^2\hat{z},0)^T \\ &= P_1(\hat{E})^3 + r_0(\hat{x}\hat{z},-\hat{y}\hat{z},0)^T + r_1(2\hat{x}\hat{y},-\hat{y}^2,0)^T \\ &\quad + s_0(0,\hat{x}\hat{y},-\hat{x}\hat{z})^T + s_1(0,2\hat{y}\hat{z},-\hat{z}^2)^T \\ &\quad + t_0(-\hat{x}\hat{y},0,\hat{y}\hat{z})^T + t_1(-\hat{x}^2,0,2\hat{x}\hat{z})^T \end{aligned} \tag{28}$$

$$\hat{W}(\hat{E}) = P_0(\hat{E}) \tag{29}$$

$$\begin{aligned} \hat{V}^*(\hat{E}) &= BDDF_1(\hat{E}) + r_2 curl(0,0,\hat{x}^2\hat{z})^T + r_3 curl(0,0,\hat{x}^2\hat{y}\hat{z})^T \\ &\quad + s_2 curl(\hat{x}\hat{y}^2,0,0)^T + s_3 curl(\hat{x}\hat{y}^2\hat{z},0,0)^T \\ &\quad + t_2 curl(0,\hat{y}\hat{z}^2,0)^T + t_3 curl(0,\hat{x}^2\hat{z},0)^T \\ &= BDDF_1(\hat{E}) + r_2(0,-2\hat{x}\hat{z},0)^T + r_3(\hat{x}^2\hat{z},-2\hat{x}\hat{y}\hat{z},0)^T \\ &\quad + s_2(0,0,-2\hat{x}\hat{y})^T + s_3(0,\hat{x}\hat{y}^2,-2\hat{x}\hat{y}\hat{z})^T \\ &\quad + t_2(-2\hat{y}\hat{z},0,0)^T + t_3(-2\hat{x}\hat{y}\hat{z},0,\hat{y}\hat{z}^2) \end{aligned} \tag{30}$$

The mixed finite element spaces on a physical element is mapped from a reference using the Piola and scalar transformations (31).

$$\begin{aligned} v \leftrightarrow \hat{v} : \hat{v} &= \frac{1}{J_E} DF_E \hat{v} \circ F_E^{-1} \\ w \leftrightarrow \hat{w} : w &= \hat{w} \circ F_E^{-1} \end{aligned} \tag{31}$$

where F_E denotes mapping from $\hat{E}$ to E; DF_E and J_E are the Jacobian and the determinant of F_E, respectively. The discrete finite element spaces V_h and W_h on τ_h are given by,

$$\begin{aligned} V_h &\equiv \{v \in V : v|_E \leftrightarrow \hat{v}, \hat{v} \in \hat{V}(\hat{E}), \forall E \in \tau_h\}, \\ W_h &\equiv \{w \in W : v|_E \leftrightarrow \hat{w}, \hat{w} \in \hat{w}(\hat{E}), \forall E \in \tau_h\}, \end{aligned} \tag{32}$$

where $H(div;\Omega) \equiv \{v \in (L^2(\Omega))^3 : \nabla \cdot v \in L^2(\Omega)\}$.

4.2 Quadrature rule

For q, v $\in V_h^*$ the local (on element E) and global (on domain Ω) quadrature rules are given by Eqs. 33–35, respectively. Where Eqs. 33 and 34 give the symmetrical and non-symmetrical quadrature rules. The non-symmetrical quadrature rules have been shown to have convergence properties for general hexahedra by [34].

$$\begin{aligned} (K^{-1}q, v)_{Q,E} &= \frac{1}{2^d} \sum_{i=1}^{2^d} J_E(\hat{r}_i)(DF_E^{-1})^T(r_i) DF_E^T(r_i) \\ &\quad K_E^{-1}(F_E(\hat{r}_i)) q(r_i) \cdot v(r_i) \end{aligned} \tag{33}$$

$$\begin{aligned} (K^{-1}q, v)_{Q,E} &= \frac{1}{2^d} \sum_{i=1}^{2^d} J_E(\hat{r}_i)(DF_E^{-1})^T(r_i) DF_E^T(\hat{r}_{c,\hat{E}}) \\ &\quad \bar{K}_E^{-1} q(r_i) \cdot v(r_i) \end{aligned} \tag{34}$$

$$(K^{-1}q, v)_Q \equiv \sum_{E \in \tau_h} (K^{-1}q, v)_{Q,E} \tag{35}$$

Here, $\hat{r}_i$ is the vertex of the reference element $\hat{E}$, $\hat{r}_{c,\hat{E}}$ is the center of mass of $\hat{E}$, $\bar{K}_E$ is the mean of K on E.

4.3 Weak formulation

We now consider the fully discrete variational formulation of the compositional flow model. The variables are taken at the most recent time iterate level everywhere except whenever explicitly indicated by index n. A sequential implicit approach is used to solve equations in pressure (p_{ref}) and concentration (N_i) variables. The pressure and concentration equations are discretized in time using a backward Euler scheme. The discrete variational problem for reservoir pressure then reads: Given $N_{i,h}^n \in W_h$ and $p_{\text{ref},h}^n \in W_h$, find $N_{i,h}^{n+1} \in W_h$, $F_{i,h}^{n+1} \in V_h$ and $p_{\text{ref},h}^{n+1} \in W_h$ such that,

$$\begin{aligned} &\left\langle \frac{1}{\Lambda_{i,h}(p_{ref}, \vec{N}_{HC})} K^{-1} F_{i,h}, v_h \right\rangle_{Q,E} - \left(p_{\text{ref},h}, \nabla \cdot v_h\right)_E \\ &= -\int_{\partial E \cap \partial\Omega} p_{\text{ref}} v_h \cdot n - \left(\frac{1}{\Lambda_{i,h}} \sum_{\alpha \neq \text{ref}} \rho_{\alpha,h} \xi_{i\alpha,h} \lambda_{\alpha,h} \nabla p_{c\alpha,h}, v_h \right)_E \\ &+ \left(\frac{1}{\Lambda_{i,h}} \sum_{\alpha} \left(\rho_{\alpha,h}^2\right) \xi_{i\alpha,h} g, v_h \right)_E, \end{aligned} \tag{36}$$

$$\left(\frac{\phi_h N_{i,h}}{\Delta t}, w_h\right)_E + \left(\nabla \cdot F_{i,h}, w_h\right)_E - \left(\nabla \cdot \sum_\alpha \left\{\phi_h S_{\alpha,h} D_{i\alpha,h} \cdot \nabla\left(\rho_{\alpha,h}\xi_{i\alpha,h}\right)\right\}, w_h\right)_E = \left(q_{i,h}, w_h\right) + \left(\frac{\phi^n N_i^n}{\Delta t}, w_h\right)_E. \quad (37)$$

$$\frac{N_w}{\rho_w} + \left(\frac{1-\nu}{\rho_o} + \frac{\nu}{\rho_g}\right)\sum_{i=2}^{N_c} N_i = 1 \quad (38)$$

Equations 36–38 constitute ($2\times N_c$+1) equations in variables p_{ref} (1 variable), N_i (N_c variables), and F_i (N_c variables). Please note that all terms, in the equations above, are at the current time level $(n+1)$ unless stated otherwise with a superscript n.

4.4 Treatment of diffusion/dispersion

The diffusion-dispersion tensor is the sum of molecular diffusion and hydrodynamic dispersion given by:

$$D_{i\alpha} = D_{i\alpha}^{\text{mol}} + D_{i\alpha}^{\text{hyd}}, \quad (39a)$$

$$D_{i\alpha}^{\text{mol}} = \tau_\alpha d_{m,i\alpha} I, \quad (39b)$$

$$D_{i\alpha}^{\text{hyd}} = d_{t,\alpha}|v_\alpha| I + \left(d_{l,\alpha} - d_{t,\alpha}\right) v_\alpha v_\alpha^T / |v_\alpha|. \quad (39c)$$

Here, τ_α is the tortuousity of phase α, $d_{m,i\alpha}$, $d_{l,\alpha}$, $d_{t,\alpha}$ are the molecular, longitudinal, and transverse dispersion coefficients, respectively. We define the diffusive/dispersive flux as:

$$J_{i\alpha} = \phi S_\alpha D_{i\alpha} \rho_\alpha \cdot \nabla\left(\xi_{i\alpha}\right), \quad (40)$$

$$\left\langle \frac{1}{\phi\rho_\alpha S_\alpha} D_{i\alpha}^{-1} J_{i\alpha}, v_h \right\rangle_{Q,E} - \left(\xi_{i\alpha}, \nabla \cdot v_h\right)_E = -\int_{\partial E \cap \partial\Omega} \xi_{i\alpha} v_h \cdot n. \quad (41)$$

The diffusion-dispersion tensor is evaluated locally for each corner-point similar to the permeability tensor. The molecular diffusion ($D_{i\alpha}^{\text{mol}}$) is evaluated using cell-centered values of $d_{m,i\alpha}$. Furthermore, the hydrodynamic dispersion tensor ($D_{i\alpha}^{\text{hyd}}$) is calculated using the three flux degrees of freedom associated with each corner-point.

5 Linearization

A Newton method is applied to form a linear system of equations followed by elimination of component concentrations and fluxes resulting in an implicit pressure system. Linearizing the above system of equations,

$$\left\langle \frac{1}{\Lambda_{i,h}(p_{ref}^k, \vec{N}^k)} K^{-1} \delta F_{i,h}, v_h \right\rangle_{Q,E} - \left(\delta p_{\text{ref},h}, \nabla \cdot v_h\right)_E = -R_{3i}^k, \quad (42)$$

$$\left(\frac{\phi_h(p_{ref}^k)}{\Delta t}\delta N_{i,h}, w_h\right)_E + \left(\frac{c_r \phi_0 N_{i,h}^k}{\Delta t}\delta p_{\text{ref},h}, w_h\right)_E + \left(\nabla \cdot \delta F_{i,h}, w_h\right)_E = -R_{4i}^k. \quad (43)$$

The local mass matrix and right-hand side for component i can be written as,

$$\begin{pmatrix} A_i^k & B & 0 \\ B^T & C_i^k & D_i^k \end{pmatrix} \begin{pmatrix} \delta F_i \\ \delta p_{\text{ref}} \\ \delta N_i \end{pmatrix} = \begin{pmatrix} -R_{3i}^k \\ -R_{4i}^k \end{pmatrix}. \quad (44)$$

Here, C_i and D_i are diagonal matrices corresponding to the first and second terms in Eq. 44. Also the Newton increment for a variable vector $\vec{x}$ is given by,

$$\delta x = \vec{x}^{k+1} - \vec{x}^k. \quad (45)$$

Eliminating δF_i in favor of cell centered quantities δp_{ref} and δN_i.

$$\left(C_i^k - B^T (A_i^{-1})^k B\right)\delta p_{ref} + D_i^k \delta N_i = -R_{4i}^k + B^T (A_i^{-1})^k R_{3i}^k \quad (46)$$

The RR Eq. 21, iso-fugacity criteria Eq. 22, and saturation constraint Eq. 38 can be linearized in terms of the unknowns p_{ref}, N_i, K_i^{par} and ν using Eqs. 17 and 20 as,

$$\sum_\alpha \left(\frac{\partial S_\alpha}{\partial p_{\text{ref}}}\right)^k \delta p_{\text{ref}} + \sum_\alpha \sum_i \left(\frac{\partial S_\alpha}{\partial N_i}\right)^k \delta N_i + \sum_\alpha \sum_i \left(\frac{\partial S_\alpha}{\partial ln K_i^{\text{par}}}\right) \delta ln K_i^{\text{par}} + \sum_\alpha \left(\frac{\partial S_\alpha}{\partial \nu}\right)^k \delta\nu = 1 - \sum_\alpha S_\alpha^k = -R_5^k, \quad (47)$$

$$\Phi_{i\alpha} = \Phi_{i\alpha}(p_{\text{ref}}, \xi_{i\alpha}) = \Phi_{i\alpha}(p_{\text{ref}}, z_i, K_i^{\text{par}}) = \Phi_{i\alpha}(p_{\text{ref}}, N_i, K_i^{\text{par}}), \tag{48}$$

$$\left(\frac{\partial ln\Phi_{io}}{\partial p_{\text{ref}}}\right)^k \delta p_{\text{ref}} + \sum_{j=2}^{N_c}\left(\frac{\partial ln\Phi_{io}}{\partial N_j}\right)^k \delta N_j + \sum_{j=2}^{N_c}\left(\frac{\partial ln\Phi_{io}}{\partial lnK_j^{\text{par}}}\right)^k \delta lnK_j^{\text{par}} + \left(\frac{\partial ln\Phi_{io}}{\partial \nu}\right)^k \delta\nu - \left(\frac{\partial ln\Phi_{ig}}{\partial p_{\text{ref}}}\right)^k \delta p_{\text{ref}} - \sum_{j=2}^{N_c}\left(\frac{\partial ln\Phi_{ig}}{\partial N_j}\right)^k \delta N_j - \sum_{j=2}^{N_c}\left(\frac{\partial ln\Phi_{ig}}{\partial lnK_j^{\text{par}}}\right)^k \delta lnK_j^{\text{par}} - \left(\frac{\partial ln\Phi_{ig}}{\partial \nu}\right)^k \delta\nu - \sum_{j=2}^{N_c}\left(\frac{\partial lnK_i^{\text{par}}}{\partial lnK_j^{\text{par}}}\right)^k \delta lnK_j^{\text{par}} = -R_{6i}^k. \tag{49}$$

The above equations can also be written in the matrix form as,

$$\begin{pmatrix} E^k & Fk & G^k & H^k \\ I^k & J^k & K^k & L^k \\ 0 & N^k & O^k & P^k \end{pmatrix} \begin{pmatrix} \delta p_{\text{ref}} \\ \delta N \\ \delta lnK^{\text{par}} \\ \delta\nu \end{pmatrix} = \begin{pmatrix} -R_5^k \\ -R_6^k \\ -R_7^k \end{pmatrix}. \tag{50}$$

We then construct the pressure equation by further eliminating δN and δlnK^{par}. Eliminating δF, δN, and δlnK^{par} from the above linear system of equations results in an implicit pressure system. Once the pressure increments (δp_{ref}) are evaluated, the concentration increments (δN_i) are obtained by back solving the linear system. Figure 1 shows a flow chart of the sequential implicit scheme used in this work. The corresponding Newton iterate level is represented by the index k.

The values of phase compressibilities (Z_α) are evaluated explicitly given pressure p_{ref}, temperature T, and component concentrations N_is. The derivatives of Z_α with respect to p_{ref} and N_i are therefore set to zero in the Jacobian. The Z_α contribution is accounted for in the residual term. A more rigorous treatment would be to expand the Jacobian in terms of Z_α as well. However, the minimum Gibbs free energy constraint (for a unique Z_α) given by Eq. 27 is difficult to utilize.

6 Results

In this section, we present numerical experiments to verify and demonstrate the capabilities of MFMFE discretization scheme for compositional flow modeling. We begin with a verification case where a comparison is made between TPFA and MFMFE discretization schemes for matching conditions. This is followed by two 2D numerical experiments, for a quarter five-spot well pattern, with homogeneous and heterogeneous permeability fields. The heterogeneous case uses a checker-board pattern permeability field to demonstrate differences in fluid front resolution for the TPFA and MFMFE scheme. Furthermore, a 2D fluvial river bed example is presented to show the effect of permeability anisotropy and reservoir geometry representation on the sweep pattern. Finally, we present numerical simulations for gas flooding of Frio and Brugge fields to demonstrate MFMFE capability to capture general reservoir geometries and field scale representation. For all the results below, a Newton tolerance of (ϵ) 10^{-8} is used with average Newton iterations (k) of 2-4 for a typical time-step sizes of 0.25–1.0 days. Please note that the values of k and time-step sizes are problem dependent and therefore the previous statement is highly subjective.

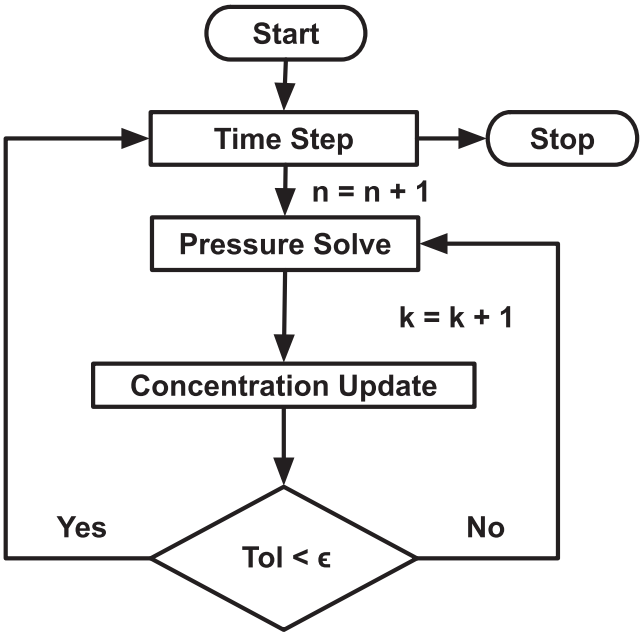

Fig. 1 Sequential implicit scheme

6.1 Verification and benchmarking

Here, we present a comparison between TPFA and MFMFE discretizations with a diagonal permeability tensor. A quarter five spot pattern with three components (C_1, C_6, and C_{20}) in addition to the water component. Both the injection (bottom left corner) and production (top right corner, Fig. 2) wells are bottom hole pressure specified with a

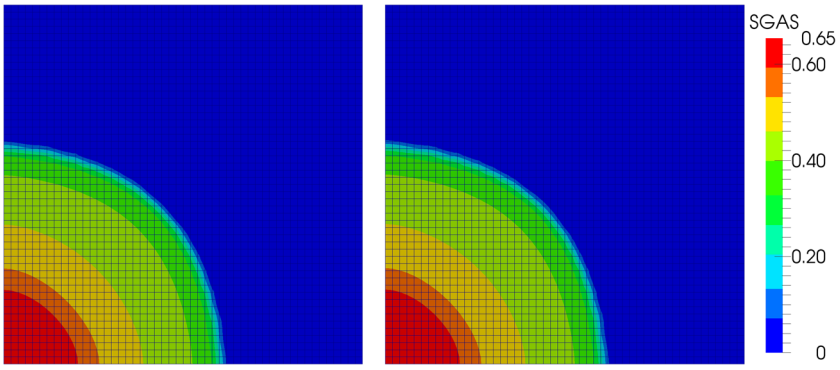

Fig. 2 Oil saturation profile after 500 days using TPFA (*left*) and MFMFE (*right*) discretizations

pressure specification of 1200 and 900 psi, respectively. The injection composition is kept constant at 100 % C_1 with reservoir and grid block dimensions of 1000 ft × 1000 ft × 20 ft and 20 ft × 20ft × 20ft, respectively. The initial reservoir pressures and water saturations are 1000 psi and 0.2, respectively. A homogeneous, isotropic, and diagonal permeability tensor field of 50 mD was assumed with a homogeneous porosity field of 0.3. The temperature was kept constant at 160 °F.

Figure 3 shows variation of component concentrations along the line joining injector and producer for both TPFA and MFMFE discretizations.

6.2 2D Homogeneous case

Here, we present a comparison between TPFA and MFMFE discretization schemes on a quarter five spot well pattern. The injector and producer are located at diagonally opposite corners in the bottom left and top right corners, respectively. The reservoir and fluid property information is kept the same as in the previous example differing only in permeability values. A homogeneous, isotropic permeability field of 100 mD is assumed with small off diagonal permeability values of 0.5 mD to construct a full permeability tensor for the MFMFE scheme. The injection (bottom left corner) and production (top right corner) wells are bottom hole pressure specified with a pressure specification of 2200 and 900 psi, respectively. Figure 4 shows the oil saturation profiles after 100 days of gas (100 % C_1) injection. The saturation profiles indicate minor differences between TPFA and MFMFE schemes using diagonal and fully permeability tensors, respectively.

6.3 2D Heterogeneous case: checkerboard pattern

This numerical experiment demonstrates the differences in saturation profiles between TPFA and MFMFE discretiza-

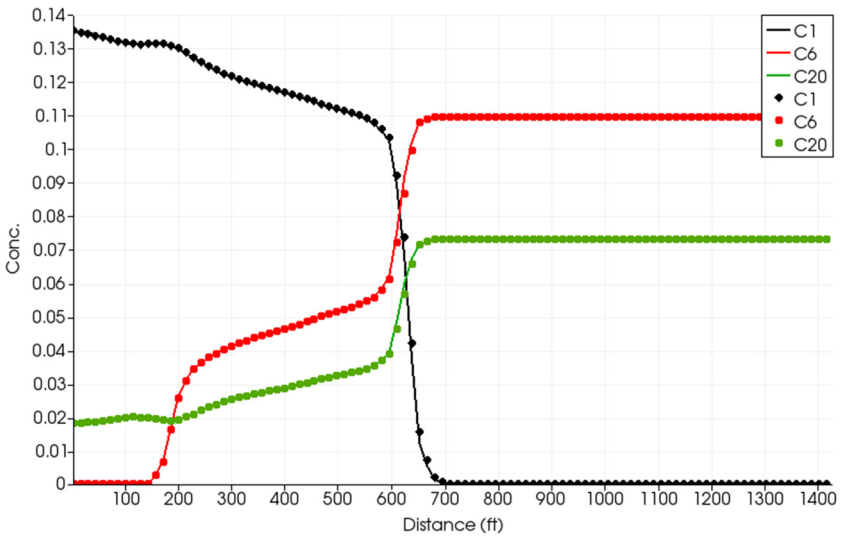

Fig. 3 Component concentrations along the injector-producer line after 500 days for TPFA (*solid-line*) and MFMFE (*dots*) discretizations

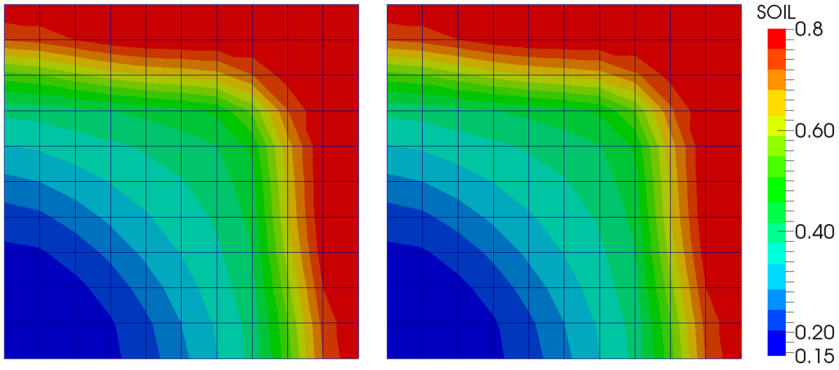

Fig. 4 Gas saturation profiles after 100 days for TPFA (*left*) and MFMFE (*right*) discretizations

tions owing to fully permeability tensor. The reservoir, fluid property, and transient information is kept the same as in the previous example differing only in permeability values. A checkerboard permeability field, as shown in Fig. 5 (left), is taken with values of 1 mD (blue) and 100 mD (red) to exaggerate the effect of heterogeneity. Additionally, small off diagonal permeability values of 0.5 mD were taken to construct a full permeability tensor for the MFMFE scheme. Figure 5 also shows the gas saturation profiles for the two discretization schemes after 3000 days. The differences in saturation profiles are significant when compared to the homogeneous case (Fig. 4). The MFMFE scheme is able to identify the high permeability diagonal direction allowing better resolution of pressure and saturations at the fluid front. The differences are more pronounced as we go from first contact miscible, multi-contact miscible to immiscible gas flooding cases.

6.4 2D Anisotropic case: fluvial river bed deposit

A simple 2D fluvial river bed deposit is considered which has a curved geometry as shown in Fig. 6. The purpose of this numerical experiment is two fold: (1) to capture the reservoir geometry and (2) to show differences resulting from representing the permeability anisotropy as a diagonal and full permeability tensor for TPFA and MFMFE schemes, respectively. The sandstone reservoirs are formed from river bed deposits consolidating over time owing to chemical and mechanical processes. These formations often exhibit a permeability anisotropy with maximum and minimum horizontal permeabilities parallel and orthogonal to the flowing river direction, respectively.

The permeability fields in such reservoirs is most accurately represented by a full tensor which rotates in a continuous fashion (Fig. 6, left) as we move upstream or downstream from a point or reference. A permeability field is generated by assuming a diagonal permeability tensor with $K_x = 100$ mD and $K_y = 10$ mD at the top left corner. A rotation of 90° is applied in small increments as we move from top left corner to the middle of the stream and back to 0 degrees at the bottom right corner. Figure 6 (middle and right) shows variations in x and y direction permeabilities along the river bed. The homogeneous reservoir porosity of 0.3 is also assumed.

The injection and production wells are placed at the top left and bottom right of the S-shaped reservoir. Furthermore, a bottom hole pressure specification of 3500 and 3000 psi

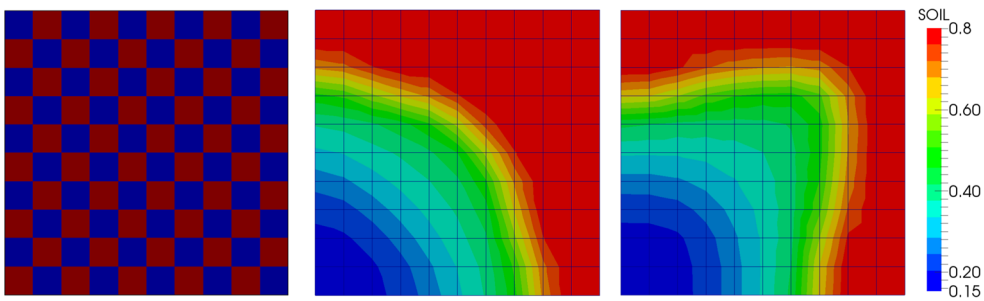

Fig. 5 Permeability field (*left*) and gas saturation profiles after 3000 days for TPFA (*middle*) and MFMFE (*right*) discretizations

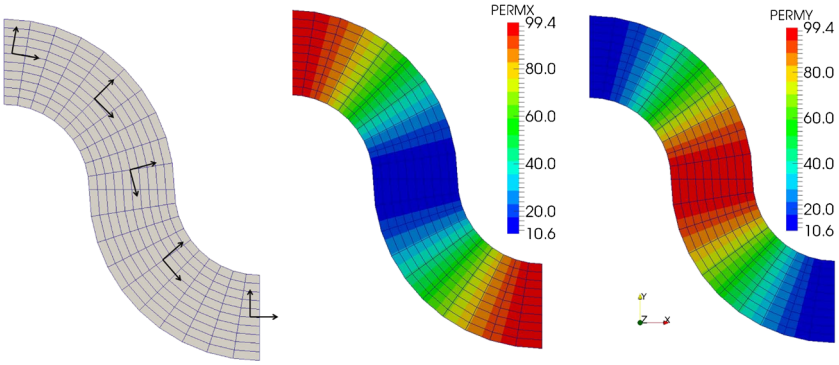

Fig. 6 X and Y direction permeabilities

was used for the injector and producer, respectively. An in situ hydrocarbon fluid composition of (0 % C_1, 10 % C_6, 20 % C_{10}, 10 % C_{15}, and 60 % C_{20}) was assumed along with an initial water saturation of 0.2. The hydrocarbon fluid composition for the gas injection well was kept constant at 100 % CH_4.

Figure 7 shows the oil saturation and CH_4 concentration profiles after 1000 days for the finite-difference (TPFA) and MFMFE scheme, respectively. Please note that the finite difference scheme requires three times the number of elements for the MFMFE discretization to effectively capture the problem geometry. Figure 8 shows a comparison of saturation and concentration profiles after 5000 days. The results clearly show differences in sweep pattern which effect hydrocarbon recoveries resulting from differences in representation of permeability ansitropy. Figure 8 also shows that compared to the MFMFE scheme, the finite difference scheme with the diagonal permeability

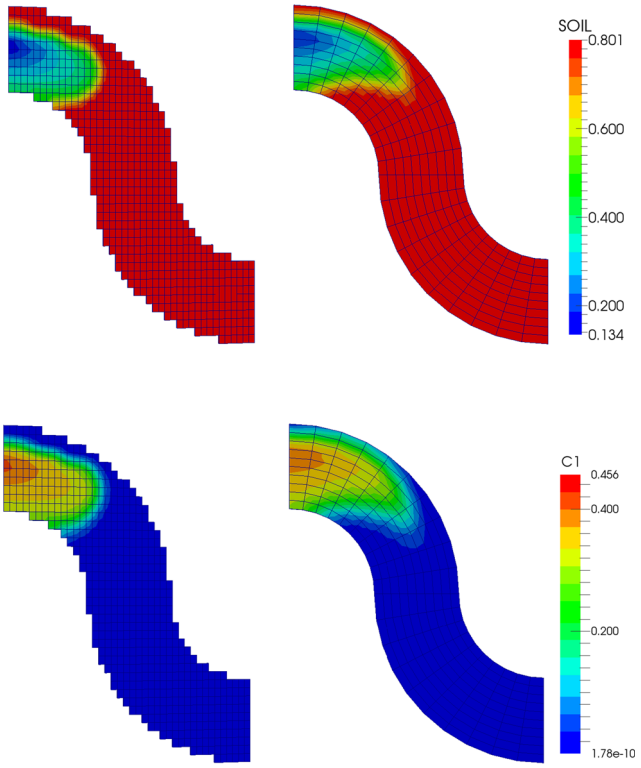

Fig. 7 Oil saturation (*top*) and CO_2 concentration profile (*bottom*) after 1000 days for TPFA (*left*) and MFMFE (*right*) discretizations

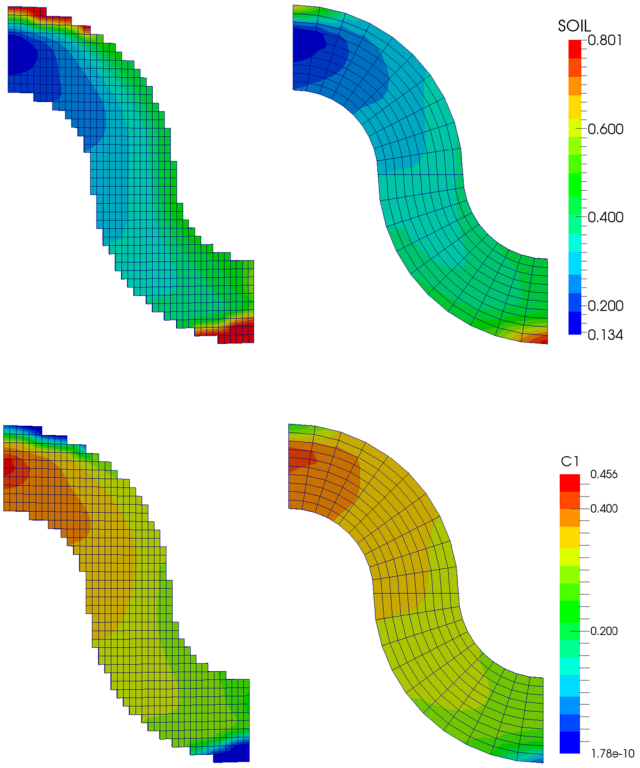

Fig. 8 Oil saturation (*top*) and CO_2 concentration profile (*bottom*) after 5000 days for TPFA (*left*) and MFMFE (*right*) discretizations

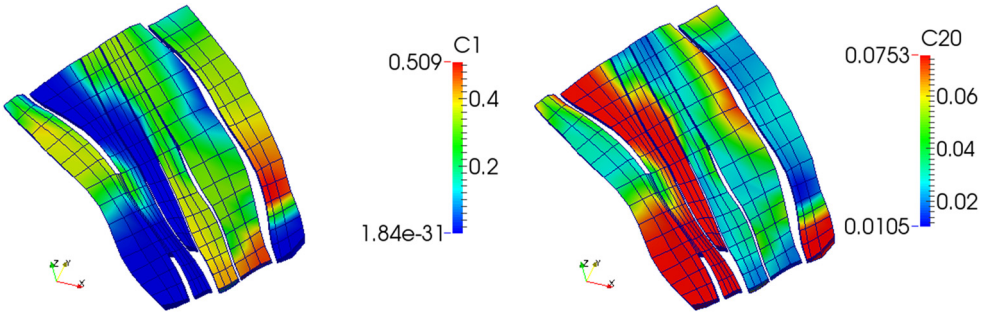

Fig. 9 Concentration profiles for lightest (C_1) and heaviest (C_{20}) components after 1000 days

tensor results in larger stagnant zones (high oil saturations) once the injection fluid breakthrough occurs at the production well.

6.5 Frio field case

In this example, we present a synthetic field case using a section of Frio field geometry information to demonstrate some of the model capabilities. Note that the general hexahedral elements allows us to capture reservoir geometry accurately without requiring substantial changes in the available petrophysical data. We consider six hydrocarbon components (C_1, C_3, C_6, C_{10}, C_{15}, and C_{20}) in addition to water forming the fluid composition. The fluid system can be at most three phases at given location, depending upon phase behavior calculations, including water, oil, and gas phases. The initial hydrocarbon composition in the reservoir is taken to be 5 % C_3, 40 % C_6, 5 % C_{10}, 10 % C_{15}, and 40 % C_{20} with an initial reservoir pressure of 2000 psi. Furthermore, the water saturation (S_w) at time $t = 0$ is taken to be 0.2. A total of eight bottom hole pressure specified wells were considered comprising of three production and five injection wells. A permeability and porosity field with typical values of 50 mD and 0.2, respectively is assumed. The injection composition was kept constant at 100 % C_1 during the entire simulation run spanning 1000 days. An isothermal reservoir condition was assumed at a temperature of 160 °F.

A multi-contact miscible (MCM) flood is achieved at the given reservoir pressure and temperature conditions. Figure 9 shows the concentration profiles for the lightest and heaviest hydrocarbon components after 1000 days. Furthermore, Fig. 10 shows the gas and oil saturation profiles after 1000 days.

6.6 Brugge field CO_2 flooding

In this example, we use CO_2 gas flooding ([5, 25]) as the tertiary mechanism for recovering hydrocarbons. The distorted reservoir geometry is captured using $9\times48\times139$ general hexahedral elements and then discretized using a MFMFE scheme. Figure 11 shows Brugge field reservoir geometry along with locations of injection and production wells. A constant temperature of 160 °F is specified assuming an isothermal reservoir condition. The initial hydrocarbon composition is 40 % (C_6) and 60 % (C_{20}) with an initial reservoir pressure of 1500 psi.

An injected gas composition of 100 % CO_2 is further specified. The figure shows the Brugge field geometry with 30 bottom-hole pressure specified wells with 10 injectors at 3000 psi and 20 producers at 1000 psi.

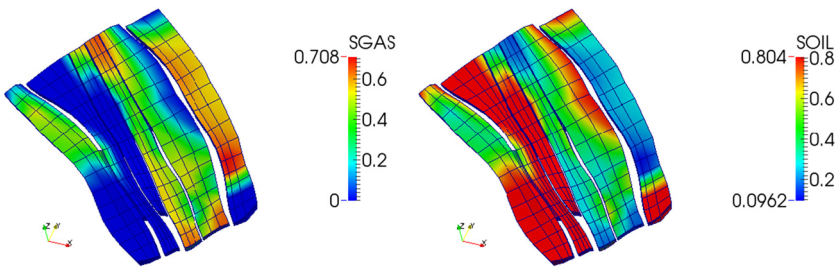

Fig. 10 Saturation profiles for gas (*left*) and oil (*right*) phases after 1000 days

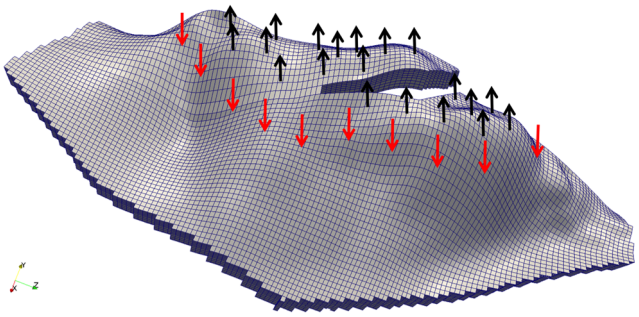

Fig. 11 Brugge field geometry with well locations

The porous rock matrix is assumed to be water wet as reflected by the relative permeability and capillary pressure curves in Figs. 12 and 13, respectively. Figure 14 shows the oil and gas saturation profile after 1000 days, whereas Fig. 15 shows the pressure distribution and concentration profiles for light (CO_2), intermediate (C_6) and heavy (C_{20}) components. A multi-contact miscible flood is achieved with miscibility occurring at the tail end of the injected gas front.

7 Conclusions

We developed a compositional flow model using MFMFE for spatial discretization. The use of general hexahedral grid leads to fewer number unknowns when compared to tetrahedral grids and therefore lower computational costs. Furthermore, the discretization scheme allows sufficient flexibility in capturing complex reservoir geometries including non-planar interfaces. The hexahedra is a plausible choice for mesh elements since reservoir petrophysical data is usually available on similar elements. An MFMFE scheme therefore facilitates adaptation with minimal changes to given information. Finally, the general compositional flow model presented here encompasses single, multi-phase and black oil flow models. This presents a future prospect for multi-model capabilities where different flow models can be used in separate reservoir domains.

Acknowledgments The authors would like to express their gratitude towards Rick Dean (ConocoPhillips) for his contributions to IPARS (Integrated Parallel Accurate Reservior Simulator) and valuable inputs.

Appendix A: Peng-robinson cubic equation of state

$$\bar{Z}_\alpha^3 - (1 - B_\alpha)\bar{Z}_\alpha^2 + \left(A_\alpha - 3B_\alpha^2 - 2B_\alpha\right)\bar{Z}_\alpha - \left(A_\alpha B_\alpha - B_\alpha^2 - B_\alpha^3\right) = 0 \quad (51a)$$

$$Z_\alpha(p_{ref}, \vec{N}_{HC}, \vec{K}^{par}, v) = \bar{Z}_\alpha(p_{ref}, \vec{N}_{HC}, \vec{K}^{par}, v) - C_\alpha \quad (51b)$$

$$A_\alpha = \sum_{i=2}^{N_c}\sum_{j=2}^{N_c} \xi_{i\alpha}\xi_{j\alpha}A_{ij} \quad (51c)$$

$$A_{ij} = (1 - \delta_{ij})(A_i A j)^{0.5} \quad (51d)$$

$$A_i = \Omega_{ai}^o \left[1 + m_i(1 - T_{ri}^{0.5})\right]^2 \frac{p_{ri}}{T_{ri}}^2 \quad (51e)$$

$$B_\alpha = \sum_{i=2}^{N_c} \xi_{i\alpha} B_i \quad (51f)$$

$$C_\alpha = \frac{P^*}{RT}\sum_{i=2}^{N_c} \xi_{i\alpha} c_i \quad (51g)$$

$$B_i = \Omega_{bi}^o \frac{p_{ri}}{T_{ri}} \quad (51h)$$

$$C_i = \frac{p_{ref}\, c_i}{RT} \quad (51i)$$

$$p_{ri} = \frac{p_{ref}}{P_{ci}} \quad (51j)$$

$$T_{ri} = \frac{T}{T_{ci}} \quad (51k)$$

$$\begin{aligned} m_i &= 0.374640 + 1.54226\omega_i - 0.26992\omega_i^2 && \text{if } \omega_i \le 0.49 \\ &= 0.379642 + 1.48502\omega_i = 0.164423\omega_i^2 + 0.016666_i^3 && \text{if } \omega_i > 0.49 \end{aligned} \quad (52)$$

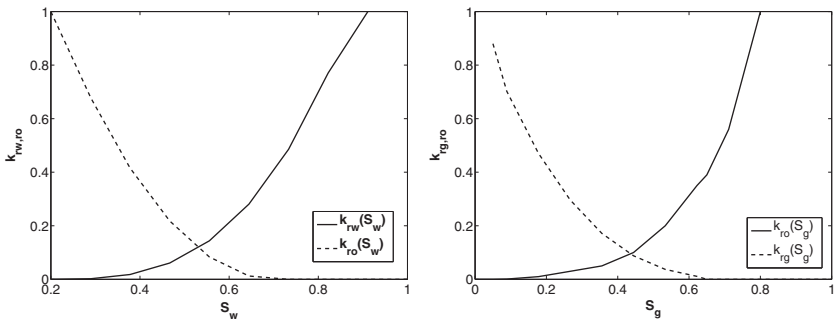

Fig. 12 Water, oil, and gas relative permeabilities

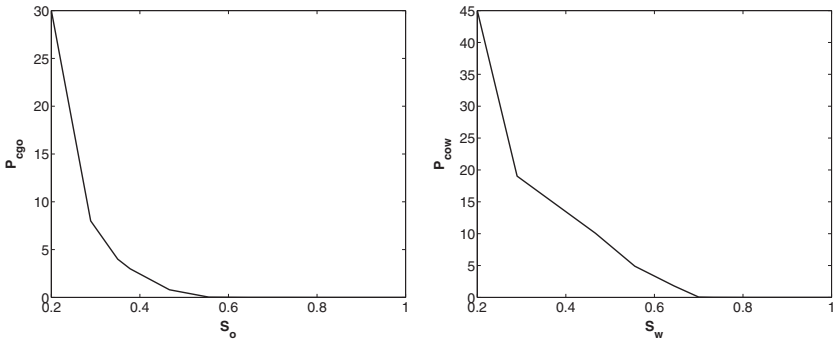

Fig. 13 Capillary pressure curves

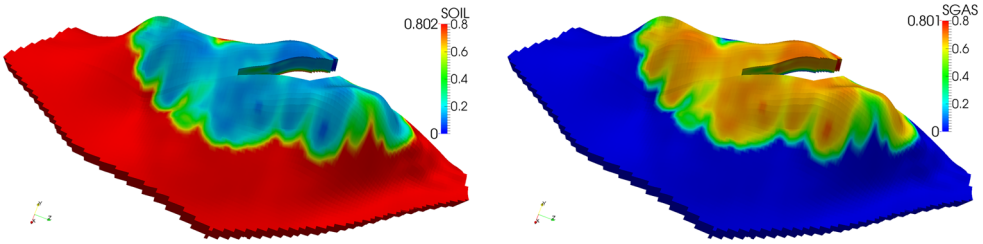

Fig. 14 Oil and gas saturation profiles after 1000 days

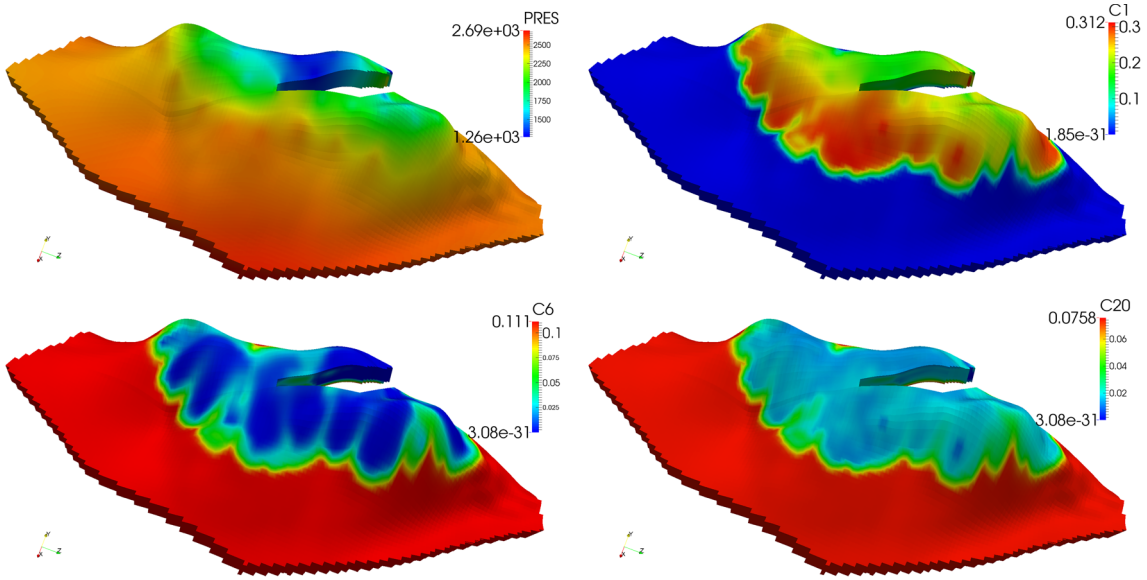

Fig. 15 Pressure and concentration profiles after 1000 days

where,

δ_{ij} = Binary interaction parameters between component 'i' and 'j' (constant).
p_{ci} = Critical pressure of component 'i' (constant).
T_{ci} = Critical temperature of component 'i' (constant).
ω_i = Accentric factor for component 'i' (constant, deviation of a molecule from being spherical).
C_α = Volume shift parameter (constant).
$\Omega^o_{a/bi}$ = Constants corresponding to the equation of state.
Z_α = Compressibility of phase 'α'.

References

1. Acs, G., Doleschall, S., Farkas, E.: General purpose compositional model. Old SPE J. **25**(4), 543–553 (1985)
2. Baker, L.E., Pierce, A.C., Luks, K.D.: Gibbs energy analysis of phase equilibria. SPE J. **22**(5), 731–742 (1982)
3. Brezzi, F., Douglas, J., Duràn, R.Jr., Fortin, M.: Mixed finite elements for second order elliptic problems in three variables. Numer. Math. **51**(2), 237–250 (1987)
4. Chang, Y.-B.: Development and application of an equation of state compositional simulator (1990)
5. Chen, C., Wang, Y., Li, G.: Closed-loop reservoir management on the brugge test case. Comput. Geosci. **14**, 691–703 (2010)
6. Coats, K.: An equation of state compositional model. Old SPE J. **20**(5), 363–376 (1980)
7. Farkas, E.: Linearization techniques of reservoir-simulation equations: fully implicit cases. SPE J. **3**(4) (1998)
8. Firoozabadi, A., Pan, H.: Fast and robust algorithm for compositional modeling: part i-stability analysis testing. SPE J. **7**(1), 79–89 (2002)
9. Fussell, L.T., Fussell, D.D.: An iterative technique for compositional reservoir models. SPE J. **19**(4) (1979)
10. Fussell, L.T.: Technique for calculating multiphase equilibria. SPE J. **19**(4), 203–210 (1979)
11. Hajibeygi, H., Tchelepi, H.A.: Compositional multiscale finite-volume formulation. SPE J. **19**(2) (2014)
12. Heidemann, R.A., Michelsen, M.L.: Instability of successive substitution. Ind. Eng. Chem. Res. **34**(3), 958–966 (1995)
13. Ingram, R., Wheeler, M.F., Yotov, I.: A Multipoint flux mixed finite element method on hexahedra. SIAM J. Numer. Anal. **48**(4), 1281–1312 (2010)
14. Kazemi, H., Vestal, C.R., Shank, D.G.: An efficient multicomponent numerical simulator. SPE J. **18**(5) (1978)
15. Lauser, A., Hager, C., Helmig, R., Wohlmuth, B.: A new approach for phase transitions in miscible multi-phase flow in porous media. Adv. Water Resour. **34**(8), 957–966 (2011)
16. Martinez, M.J., Stone, C.M.: Considerations for developing models of multiphase flow in deformable porous media. SANDIA REPORT, SAND2008-5887 (2008)
17. Mehra, R.K., Heidemann, R.A., Aziz, K.: Computation of multiphase equilibrium for compositional simulation. SPE J. **22**(1), 61–62 (1982)
18. Michelsen, M.L.: The isothermal flash problem. part i. stability. Fluid Phase Equilib. **9**(1), 1–19 (1982a)
19. Michelsen, M.L.: The isothermal flash problem. part ii. phase-split calculation. Fluid Phase Equilib. **9**(1), 21–40 (1982b)
20. Michelsen, M.L.: Calculation of multiphase equilibrium. Comput. Chem. Eng. **18**(7), 545–550 (1994)
21. Nghiem, L.X., Fong, D.K., Aziz, K.: Compositional modeling with an equation of state. SPE J. **21**(6) (1981)
22. Okuno, R., Johns, R.T., Sepehrnoori, K.: A new algorithm for rachford-rice for multiphase compositional simulation. SPE J. **15**(2), 313–325 (June 2010)
23. Pan, H., Firoozabadi, A.: Fast and robust algorithm for compositional modeling: part ii-two-phase flash computations. SPE J. **8**(4), 380–391 (2003)
24. Peng, D.-Y., Robinson, D.B.: A new two-constant equation of state. Indust. Eng. Chem. Fund. **15**(1), 59–64 (1976)
25. Peters, E., Arts, R., Brouwer, G., Geel, C.: Results of the Brugge benchmark study for flooding optimisation and history matching. SPE 119094-MS. SPE Reservoir Simulation Symposium (2009)
26. Rachford, H.H., Rice, J.D.: Procedure for use of electronic digital computers in calculating flash vaporization hydrocarbon equilibrium. Trans. Am. Instit. Min. Metall. Eng. **195**, 327–328 (1952)
27. Roebuck, I.F.Jr., Henderson, G.E., Douglas, J.Jr., Ford, W.T.: The compositional reservoir simulator: case I-the linear model. Old SPE J. **9**(01), 115–130 (1969)
28. Russell, T.F., Wheeler, M.F.: Finite element and finite difference methods for continuous flows in porous media. Math. Reserv. Simul. **1**, 35–106 (1983)
29. Singh, G., Pencheva, G., Kumar, K., Wick, T., Ganis, B., Wheeler, M.F.: Impact of Accurate Fractured Reservoir Flow Modeling on Recovery Predictions. SPE Hydraulic Fracturing Technology Conference (2014)
30. Sun, S., Firoozabadi, A.: Compositional Modeling in Three-Phase Flow for CO2 and other Fluid Injections using Higher-Order Finite Element Methods. SPE Annual Technical Conference and Exhibition (2009)
31. Thomas, S.G.: On some problems in the simulation of flow and transport through porous media. PhD. Thesis (2009)
32. Watts, J.W.: A compositional formulation of the pressure and saturation equations. SPE Reserv. Eng. **1**(3), 243–252 (1986)
33. Wheeler, M.F., Xue, G.: Accurate locally conservative discretizations for modeling multiphase flow in porous media on general hexahedra grids. Proceedings of the 12th European Conference on the Mathematics of Oil Recovery-ECMOR XII, publisher EAGE (2011)
34. Wheeler, M., Xue, G., Yotov, I.: A multipoint flux mixed finite element method on distorted quadrilaterals and hexahedra. Numer. Math. **121**(1), 165–204 (2011a)
35. Wheeler, M.F., Yotov, I.: A Multipoint flux mixed finite element method. SIAM J. Numer. Anal. **44**(5), 2082–2106 (2006)
36. Wheeler, M.F., Xue, G., Yotov, I.: A family of multipoint flux mixed finite element methods for elliptic problems on general grids. Proc. Comput. Sci. **4**, 918–927 (2011b)
37. Wilson, G.: A modified redlich-kwong equation of state applicable to general physical data calculations. Paper No15C, 65th AIChE National meeting (1968)
38. Wong, T.W., Firoozabadi, A., Aziz, K.: Relationship of the volume-balance method of compositional simulation to the Newton-Raphson method. SPE Reserv. Eng. J. **5**(3) (1990)
39. Young, L., Stephenson, R.: A generalized compositional approach for reservoir simulation. Old SPE J. **23**(5), 727–742 (1983)